

## Thomson Scattering with laser intra-cavity multi-pass system to study fast changing structures in fusion plasma

**M.Yu.Kantor<sup>1</sup>**

*FOM Institute DIFFER, 3430 BE Nieuwegein, The Netherlands*

*Ioffe Institute, Polytekhnicheskaya 26, Saint-Petersburg 191024, Russia*

*Max-Planck-Institut für Plasmaphysik, D-85748 Garching bei München, Germany*

*E-mail: m.kantor@mail.ioffe.ru*

**A. J. H. Donné**

*EUROfusion D-85748 Garching bei Munchen, Germany*

*FOM Institute DIFFER, 3430 BE Nieuwegein, The Netherlands*

*Eindhoven University of Technology, 5600 MB Eindhoven, The Netherlands*

*E-mail: Tony.Donne@euro-fusion.org*

### ABSTRACT

Advanced Thomson Scattering (TS) diagnostics with a Laser Intra-cavity Multi-pass Probing (LIMP) system were developed and implemented in several tokamaks in recent decades. The LIMP system provides a significant gain of the laser probing energy along with generation of many pulses at a high repetition rate within a single pumping pulse. Probing lasers with a LIMP system have considerably extended the capability of the TS diagnostic and have opened new application fields in plasma physics.

The paper presents the principles of the LIMP system which underlie its efficiency as well as some of its applications in physical studies performed in the TEXTOR tokamak. The TS diagnostic with LIMP has enabled detailed measurements of fluctuations of electron temperature and density along the whole plasma diameter. The structure of these fluctuations, which are typically 1-2% in amplitude, has been resolved. The diagnostic made it possible to measure the fine structure of rotating magnetic islands in the TEXTOR plasma. The observed structures significantly differ from the classical shape of helical magnetic perturbations.

LIMP is applied for measurements of not only electrons but also of other plasma particles. Laser-heated dust micro-particles were detected in plasma via their thermal radiation. The diagnostic provides the location of particles along with its velocity, temperature and dimension.

The measurement principles and a discussion of the results are presented in the paper.

*First EPs Conference on Plasma Diagnostics - 1<sup>st</sup> ECPD*

*14-17 April 2015,*

*Villa Mondragone, Frascati (Rome) Italy*

## **1.Introduction**

Thomson scattering (TS) is a straightforward and reliable method of measuring electron temperature and density and is widely used in fusion studies. The very small cross-section of Thomson scattering limits the diagnostic sensitivity, spatial resolution and sample rate of measurements and restricts the application of the diagnostic. The underlying work presents an approach which considerably improves the diagnostic capabilities and opens up new application fields.

The approach is based on the use of a Laser Intra-cavity Multi-pass Probing (LIMP) system to enhance the laser pulse probing energy as well as the repetition rate. It was developed and applied for many years in several tokamaks [1-5] to study fast plasma processes.

The developed laser system is most efficient for physical studies of fast events when it is combined with a multi-channel high resolution light detection system. Then a TS diagnostic enables studies of fast changing structures in the plasma which are inaccessible for any other diagnostic. Such a TS diagnostic with a LIMP system was developed for the TEXTOR tokamak and successfully operated in many physics programs.

The paper gives an overview of the Thomson diagnostic with LIMP system and a collection of results gathered in the TEXTOR tokamak.

## **2.Thomson scattering for measurements of fast changing structures in plasma**

### **2.1 Main technical requirements on TS diagnostic for measuring fast events in plasma**

There are many events in fusion plasmas which requires a local diagnostic operating at a high frequency and providing a high spatial resolution and accuracy of measurements in a large number of spatial points. The TS diagnostic can contribute in studies of periodic events like sawteeth, magnetic islands and Edge Localized Modes (ELMs) well as non-periodic events like disruptions and L-H transitions. The diagnostic can also be a unique instrument to study electron transport by measuring electron temperature and density profiles during heat pulse propagation in the plasma or the measure fluctuations in these parameters directly.

Most of these events have typically a time scale of 1 ms and a size of a few cm in large tokamaks. A high spatial and time resolution is required for these measurements together with a very high diagnostic accuracy, because in many cases variations of plasma parameters between successive measurements are much less than 10%.

Thus, the technical requirements to a TS diagnostic for these studies are the highest accuracy (<3%), sampling rate (~10 kHz) and spatial resolution (<1 cm) of the measurements along with large number of spatial measurement points to resolve structures in plasma. The critical issue to realize the measurement requirements is a high power probing laser.

The demanded measurement accuracy is enabled only with a laser pulse of a very high probing energy, typically much higher than 10 J, whereas standard probing lasers generate either up to 10 J (ruby) or 2 J (Nd:YAG) pulses. The pulse energy of standard lasers can hardly be increased because of overheating of the laser elements by the high pumping power with the risk of exceeding the optical damage threshold by the powerful laser beams.

The demanded sampling rate is about two orders of magnitude higher than the repetition frequency of standard Nd:YAG lasers. Their frequency can be increased only at the expense of laser pulse energy or boosting pumping power. Both ways are not acceptable in our case.

An intra-cavity multi-pass laser probing system has been developed to overcome these restrictions and enable the study of fast events in fusion plasmas.

## 2.2 LIMP system on the TEXTOR tokamak and measurement errors of the TS diagnostic

The TS diagnostic on the TEXTOR tokamak was built to study fast plasma events at a high spatial resolution [4,5]. The diagnostic is based on an intra-cavity multi-pass system with a ruby laser and fast CMOS cameras for detection of scattered light that is spectrally resolved by a grating spectrometer in the Littrow setup [3].

The CMOS cameras record scattered spectra collected from 120-160 spatial points at a spatial resolution of 5-7 mm. The intensity of spectrally resolved light is increased by a gated image intensifier. The laser multi-pass system enables generation of laser pulses with effective probing energy  $\sim 50$  J at a repetition rate of 5 kHz. A high probing energy and efficient light detection enable TS measurements with a statistical error of 1-2%.

The correct estimation of statistical errors is very important for the calculation of the electron temperature and density from scattered spectra and for a correct interpretation of the measurements results.

The errors are calculated from multiple calibrations of the diagnostic system under the assumption that statistical errors are determined by counting noise of the photoelectrons escaping from the cathode of the image intensifier.

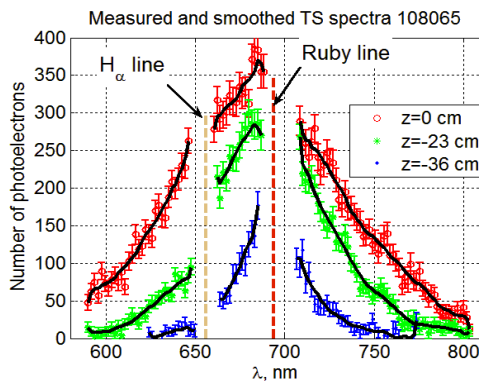


Fig. 1

TS spectra from three spatial points. Measured data are shown with symbols and error bars. Smoothed curves are shown black

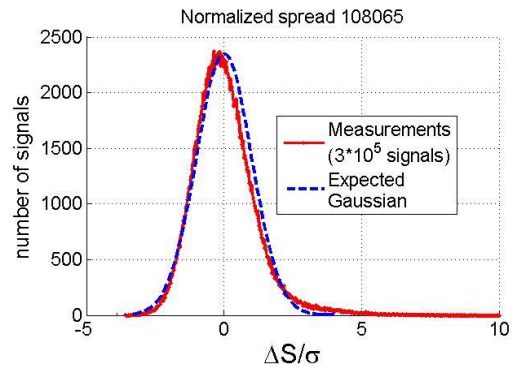


Fig. 2

Measured and expected distributions of the spread of spectral signals around the smoothed curves normalized to the error bars.

The statistical errors are verified by comparison of the predicted error bars with the spread of signals in spectral channels around the smoothed spectra. The spread calculated from TS spectra measured in 120 spatial points and for three spectra are shown in Fig. 1. The spread of the data points is the difference between the measured points and the corresponding black curves. The distribution of the spread normalized to the predicted statistical standard deviation is shown in Fig. 2 by the red curve. The plot collects  $3 \cdot 10^5$  scattered signals measured in 43 laser pulses. The mean of the normalized spread is  $-0.03$ , which is very close to the expected

zero value. The distribution of the spread is close to the expected Gaussian shape shown in the figure by the blue dashed curve.

Thus, the statistical errors of scattered signals are determined by photoelectron counting. They typically range from 5 to 20% for most spectral channels which yields a high accuracy of measurements of electron temperature and density.

### 3. Fluctuations of electron temperature and density in TEXTOR

Regression of scattered signals with Mattioli spectra [6] is used for determining the electron temperature ( $T_e$ ) and density ( $n_e$ ) as well as their statistical errors. Results of the regression analysis of TS measurements in an ohmic plasma discharge with very low MHD activity is shown in Fig. 3.

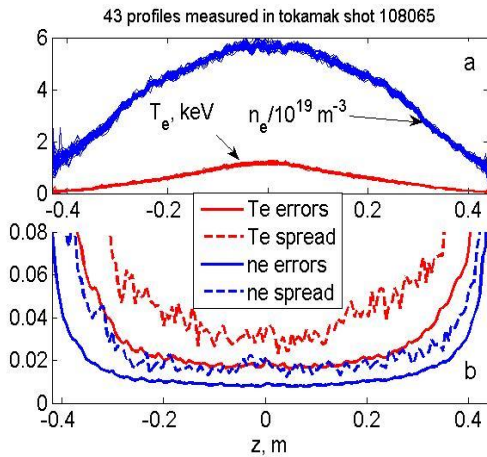


Fig 3

Profiles of  $T_e$  and  $n_e$  and their relative statistical errors

- a. 43 profiles measured in 160 spatial points
- b. Relative statistical errors and data spread

Figure 3a shows 43 measured  $T_e$  and  $n_e$  profiles, whereas the bottom plot refers the statistical measurement errors and the spread of  $T_e$  and  $n_e$  around their time averages. The diagnostic provides statistical errors of 1% and 2% correspondingly for temperature and density measurements in the plasma core. The spread of  $T_e$  and  $n_e$  data appeared to be twice as high as the statistical errors. This difference is attributed to  $T_e$  and  $n_e$  oscillations which can be separated into slow variations and fast fluctuations.

Slow variations are revealed by time smoothing the difference between the measured  $T_e$  and  $n_e$  profiles and their time averages. Fast fluctuations are unveiled by subtraction of the slow variations and time averages from the measured  $T_e$  and  $n_e$  profiles. The relative standard deviations of the slow and fast oscillations are plotted in Fig. 4. They range from 0.5% to 3% in the plasma core and increase up to the 10% level at the plasma edges. The standard deviations were calculated while taking into account the statistical measurement errors.

The structure of the slow variations shown in Fig. 5 are well resolved in space and time with less than 1% accuracy because of smoothing. They likely relate to the growth of weak sawteeth when  $T_e$  and  $n_e$  are converging to the  $q < 1$  plasma region.

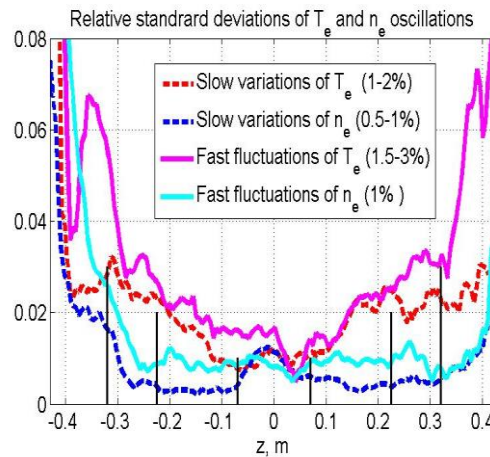


Fig. 4

Relative standard deviations of  $T_e$  and  $n_e$  oscillations.

- Positions of  $q=1, 2, 3$  surfaces are shown by vertical black lines.

The structure of the fast fluctuations is masked by measurement errors and looks more irregular. Their structure is unveiled by means of correlation analysis of the fluctuations. A normalized correlation function  $C_f(z_0, z, \tau)$  is calculated from a two dimensional function  $f(z, t)$ :

$$C_f(z_0, z, \tau) = \langle f(z_0, t) * f(z, t + \tau) \rangle / \langle f(z_0, t) * f(z, t) \rangle,$$

where brackets  $\langle \rangle$  mean time averaging,  $\tau$  is a time lag,  $z_0, z$  are spatial points and  $f$  represents either  $T_e$  or  $n_e$  fluctuations. The calculated correlations  $C_{T_e}$  and  $C_{n_e}$  of the fluctuations reveals their structures in time and space. The structures of the  $T_e$  and  $n_e$  fluctuations are presented by the correlations in Fig. 6 for  $z_0=0$  and  $\text{abs}(z) < 0.44$  m. The signal at  $z = 0$  m and  $\tau = 0$  ms was taken as reference.

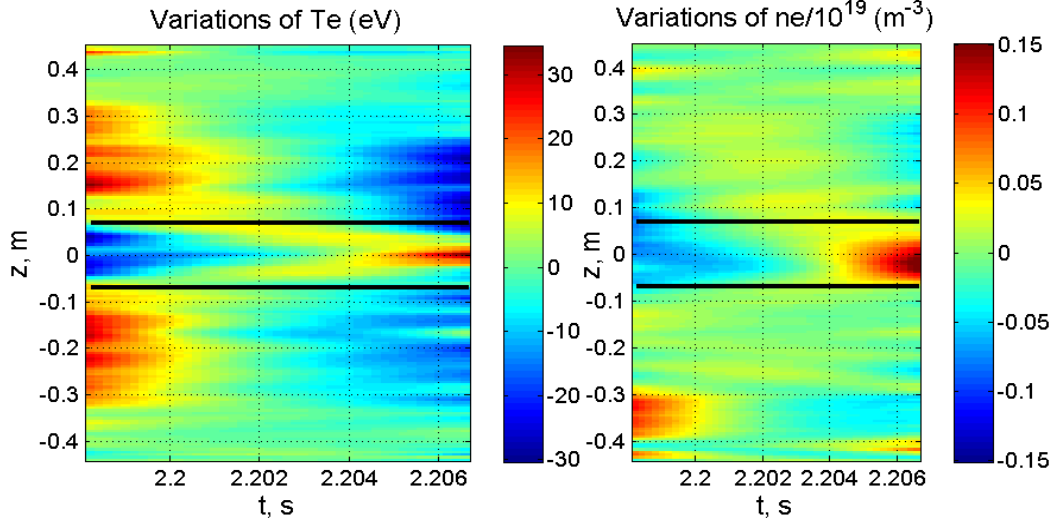


Fig. 5.

Slow variations of  $T_e$  and  $n_e$ . The black lines are the positions of  $q=1$  surface.

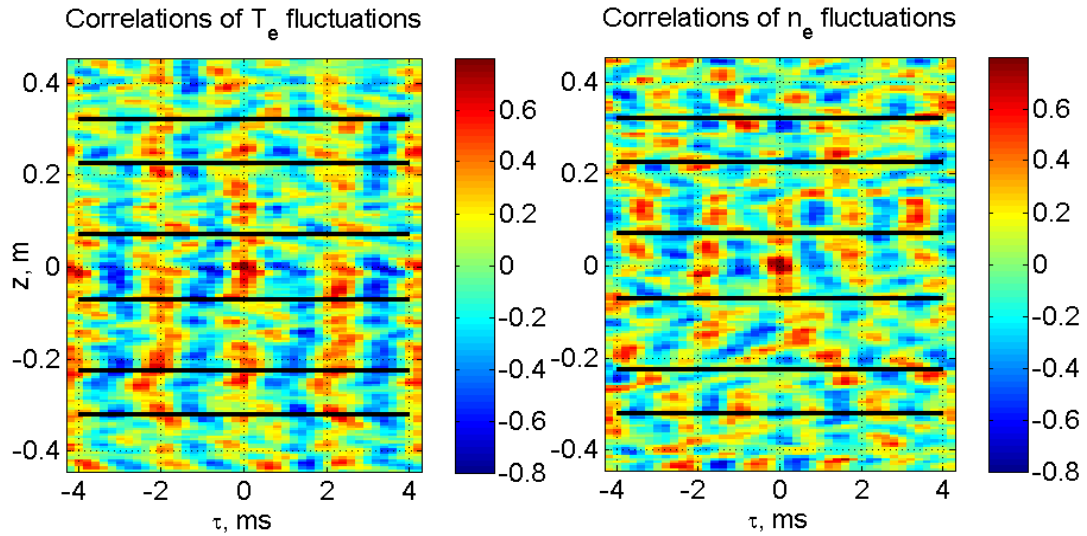


Fig. 6

Correlations of fast fluctuations of  $T_e$  and  $n_e$

The black lines are the positions of  $q=1, 2$  and  $3$  surfaces.

The horizontal axis of the plots is the time lag between two correlating values. The first of them is taken in the central point  $z_0=0$  and the second one is taken at another point at the  $z$  coordinate. The fluctuations show  $\sim 500$  Hz periodical structures which may relate to the toroidal rotation of the plasma column. The time lag between phase synchronized  $T_e$

fluctuations is less than 1 ms inside the  $q=2$  surface and gets larger towards the plasma edge. Global density fluctuations show a larger time lag between  $n_e$  fluctuations in the plasma core. The typical spatial wavelength scale of the fluctuations is 3-5 cm. More detailed structures of the fluctuations can be found from further correlation analysis of the measurements.

#### 4. Fine structure of rotating magnetic islands

Rotating islands in TEXTOR are excited by AC helical currents in the Dynamic Ergodic Divertor (DED) coils [7] wrapped around the central column of the tokamak. These currents create a perturbed magnetic field rotating in the toroidal direction at  $\sim 1$  kHz frequency and driving magnetic islands in the plasma. The TS diagnostics provides measurements of the  $T_e$  and  $n_e$  evolution along the whole plasma diameter during several periods of island rotation.

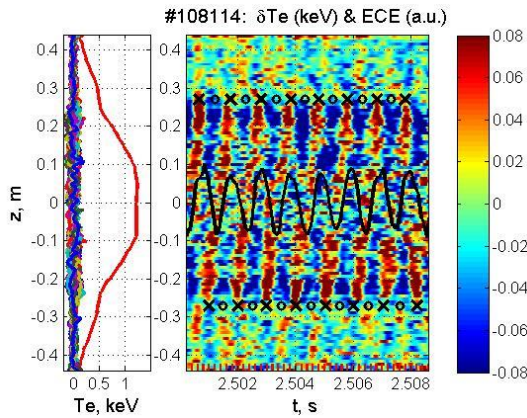


Fig. 7

$T_e$  oscillations in magnetic islands  
The black curve is a  $T_e$  oscillation from ECE

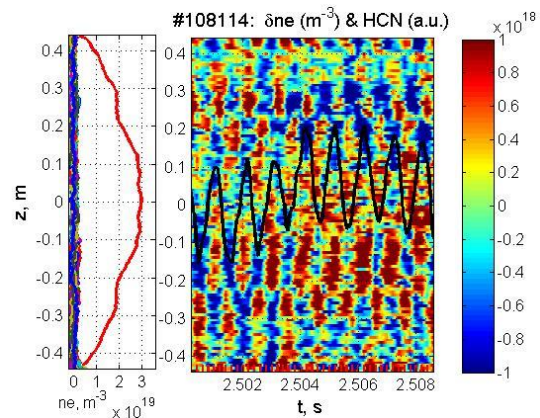
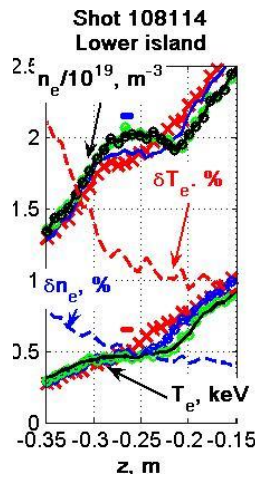


Fig. 8

$n_e$  oscillations in magnetic island  
The black curve is an  $n_e$  oscillation from interferometry

The dynamics of  $T_e$  and  $n_e$  measured by the TS diagnostic are shown in Fig. 7 and 8 [8]. The  $T_e$  and  $n_e$  profiles averaged over a 9 ms time interval are shown in the left hand sides of the figure sections along with the  $T_e$  and  $n_e$  variations in individual pulses located around the zero lines of these plots. The time-space domains of the variations are shown in the contour plots which reveal island structures with a resolution of 4 eV and  $1 \cdot 10^{17} \text{ m}^{-3}$ .



Lower island

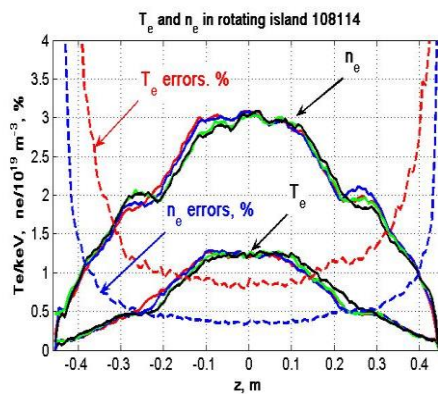
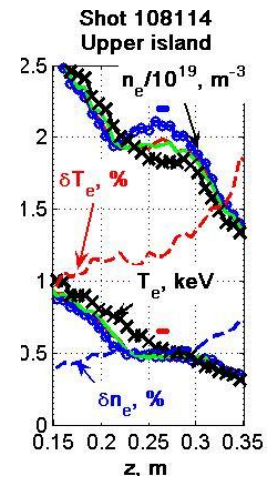


Fig. 9

$T_e$  and  $n_e$  profiles in four phases of the island.  
o-points up – blue, x-point up black,  
o-points low – green, x-point low red



Upper island

TS measurements over several periods of the island allow to improve statistical errors to values below 1% by averaging the TS data by taking into account their relative phases (boxcar averaging). This high accuracy enables to reconstruct the fine structure of the magnetic islands. The profiles of  $T_e$  and  $n_e$  in the islands when o- and x-points appear consecutively on the top and the bottom of its magnetic surface are shown in Fig. 9. The island regions are enlarged and shown in the side panels of the figure. The spatial resolution and accuracy of the  $T_e$  and  $n_e$  reconstruction are shown by colour bars above the appropriate curves in the side panels.

The structures of the island in terms of electron temperature, density and pressure are shown in Fig. 10 by contours of their constant levels distanced by  $<1\%$  of their local values. The contour shapes considerably differ from the symmetrical structure of the magnetic perturbations in classical islands [9]. The measured structures differ from the theoretical ones by elongated x-points and a considerable radial shift between the o- and x-points of the  $T_e$  and  $n_e$  islands.

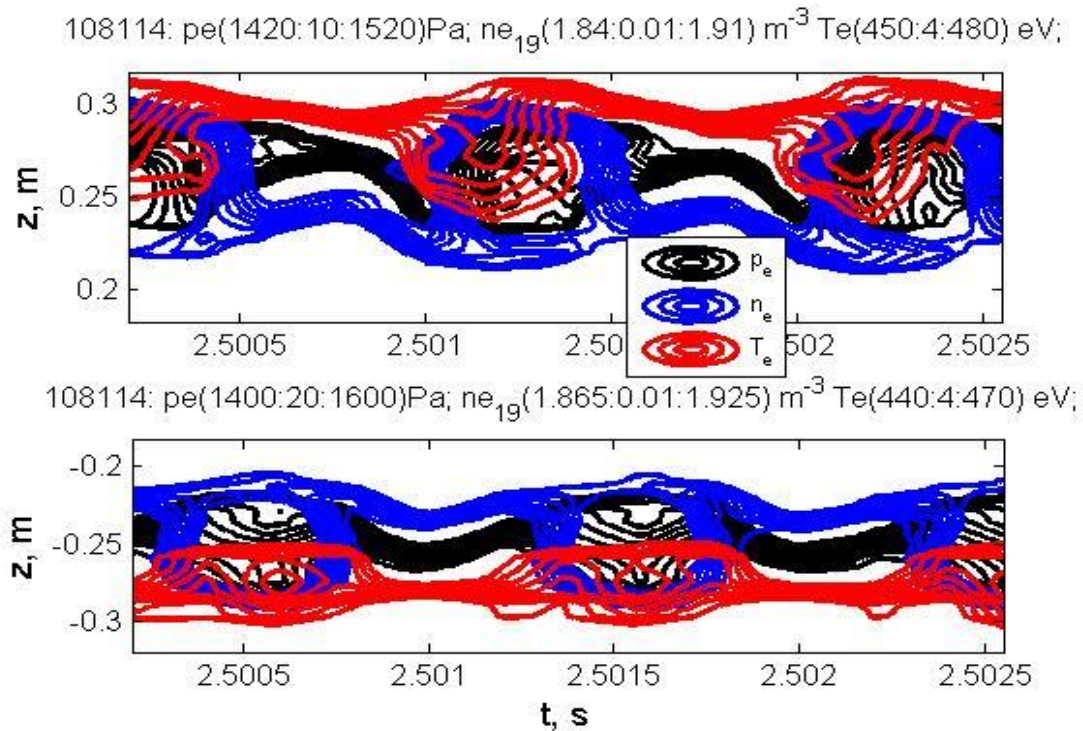


Fig. 10

Structures of electron temperature, density and pressure in magnetic island

## 5.Characterization of dust micro-particles in a plasma from their thermal emission

The LIMP system enables efficient applications of the diagnostic for studies of not only electrons but also of other plasma particles. The diagnostic was used for *in situ* characterization of dust micro-particles in the TEXTOR plasma [10]. The method is based on measuring the thermal radiation of a single micro particle heated by the laser beam or by the surrounding plasma. Laser heating makes colder particles detectable and they are localized in the intersection of the laser beam and the line of sight of the light collection system. The number density of dust particles and their velocities along the laser probing beam are deduced from the statistical analysis of the detected dust in space and time. Temperatures and size of the particles are

determined from the shape and absolute level of their thermal radiation taking into account thermal destruction of the particles.

Dust particles in tokamaks were first detected by a standard TS diagnostics with the use of Mie scattering [11]. Possibilities of such diagnostic are restricted by

- (1) a very high intensity of laser probing beams which burns small particles out before they have been detected,
- (2) a short laser pulse duration and small probing volume which reduces the sensitivity and detection probability of dust particles

Mie scattering at the laser probing wavelength causes the diagnostic to be affected by stray light. The LIMP system gives a number of advantages in terms of characterization of dust in comparison to standard TS diagnostics:

- (a) The lower laser intensity reduces destruction of dust particles during laser heating, thus improving the detection threshold and the measurement of the particle size;
- (b) the long laser pulse increases the time for collection of thermal radiation from particles which improves the sensitivity of the diagnostic;
- (c) The large cross section of the laser beams provides about a 10-fold increase in the detection probability of dust;
- (d) The high repetition rate of TS measurements allows for the detection of many dust particles and measurements of their velocities;
- (e) Spectral analysis of thermal radiation enables additional characteristics of dust particles like surface temperature and size;
- (f) The configuration for dust detection is fully compatible with standard TS measurements.

Thermal radiation from dust particles is detected as a number of broad band spectra on the background of TS spectra and plasma light (see Fig. 11). Similar thermal radiation from dust particles has been observed with the high resolution TS diagnostic on JET [12].

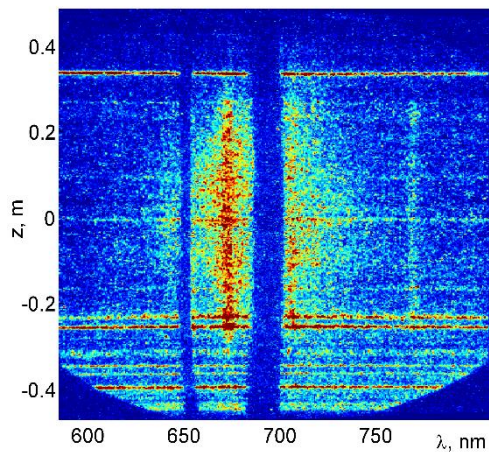


Fig. 11

Thermal radiation of dust in a wide spectral band on the background of plasma and TS light.

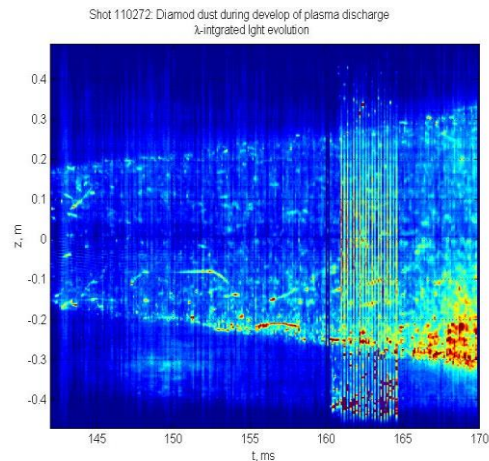


Fig. 12

Visualization of dust particles. The dust particles are seen as bright spots in the integrated spectra

Integration of spectra over the whole wavelength range provides the  $z$  positions of dust particles. They are visible in Fig. 12 as bright dots and traces in the image taken during the plasma breakdown and dust injection in TEXTOR. The laser burst is applied between 160 and

165 ms in the discharge and it highlights particles in the plasma and outside its separatrix. The total number of detected particle is more than 1000.

The analysis of particle traces in Fig. 12 provides measurements of their velocities in the direction of the probing axis. The rms velocity of the distribution is 22 m/s, whereas there are particles moving faster than 100 m/s.

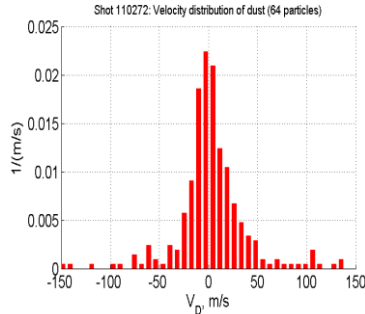


Fig 13.

Velocity distribution of dust

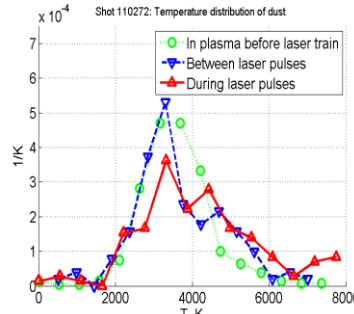


Fig 14.

Temperature distribution of dust

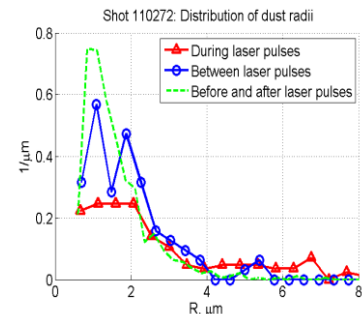


Fig 15.

Size distribution of dust particle

The dust temperature is found by fitting the measured thermal spectra to a Planck black body emission spectrum assuming constant emissivity of the dust in the spectral range of the measurements. The measured temperature distributions are shown in Fig. 14 for dust particles detected during plasma breakdown. The mean dust temperature during the laser pulses is  $\sim 4000$  K in accordance with estimations from the steady state equations in [13].

The mean temperature measured during laser pulses is about 500 K higher than that without the pulses. Laser heating of most dust particles is not pronounced in the background of their plasma heating which is in accordance with estimations in [13, 14]. A high temperature tail in Fig. 14 indicates that a small portion of dust particles can be strongly heated by simultaneous action of plasma and laser beams.

The particle size was measured from the number of the collected thermal emission photons from the particle, assuming it has a spherical shape. The calculations take into account the destruction rate of the particles which is strongly increasing with dust temperature [14].

The measured distributions of particle radii is shown in Fig. 15. The number of particles of small size ( $< 2 \mu\text{m}$ ) becomes less during laser pulses (red curve). Larger particles detected between the laser pulses could be attributed to the condensation of the ablation cloud and its re-deposition on the particle surface when the particle cooled down fast after the end of the laser pulse.

## 6. Conclusions

The Laser Intra-cavity Multi-pass system moves the TS diagnostic forward to the study of fast changing structures in fusion plasma. A TS diagnostic with LIMP in the TEXTOR tokamak was capable to detect fluctuations in the electron temperature and density at a level of 1-2% and to measure their structure in space and time. The fine structure of the temperature and density was also measured in rotating magnetic islands. The diagnostic system with LIMP has been developed not only for studying electrons but for measurements of the location, velocity, temperature and size of dust micro-particles in plasma.

## Acknowledgement

This work has been carried out within the framework of the EUROfusion Consortium and has received funding from the Euratom Research and Training Programme 2014-2018 under grant agreement No 633053. The views and opinions expressed herein do not necessarily reflect those of the European Commission.

## References

- [1] M. Yu. Kantor and D. V. Kouprienko, *High repetition rate probing laser for Thomson scattering diagnostics*, Rev. of Scient. Instr. **70**, 1 (780), 1999
- [2] M. Yu. Kantor et al., *Test of a periodic multipass-intracavity laser system for the TEXTOR multiposition Thomson scattering diagnostics*. Rev. of Scient. Instr. **72**, 1 (1159), 2001
- [3] H. J. van der Meiden et al., *10 kHz repetitive high-resolution TV Thomson scattering on TEXTOR*. Rev. of Scient. Instr. **75**, (3849), 2004
- [4] M. Yu. Kantor et al., *Thomson scattering system on the TEXTOR tokamak using a multi-pass laser beam configuration*. Plasma Phys. Control. Fusion **51** (055002), 2009
- [5] M. Yu. Kantor et al., *Thomson scattering diagnostic for study fast events in the TEXTOR plasma*. In proceedings of 36th EPS and Plasma. Phys. ECA Vol.33E, Sofia, Bulgaria, P1.184, 2009.
- [6] M. Mattioli. *Incoherent light scattering from high temperature plasmas*. EUR-CEA-FC-752, 1974
- [7] Special Issue, Fusion Eng. Design 37 (335), 1997, edited by K.H. Finken
- [8] M. Yu. Kantor et al., *Fine structure and dynamics of rotating magnetic islands in the TEXTOR tokamak*. In proceedings of 37th EPS and Plasma. Phys. ECA Vol.34A, Dublin, Ireland, P4.134, 2010.
- [9] R. Fitzpatrick, *Helical temperature perturbations associated with tearing modes in tokamak plasmas*. Phys. Plasmas **2** (825), 1995
- [10] M. Yu. Kantor et al. *Characterization of dust particles in the TEXTOR tokamak with Thomson scattering diagnostic*. Journ. Nucl. Materials. **438** (711) 2013
- [11] W.P. West et al., *Measurement of number density and size distribution of dust in DIII-D during normal plasma operation*. Plasma Phys. and Contr. Fusion, 48 (1661), 2006
- [12] E. Giovannozzi et al., *Detection of dust on JET with the high resolution Thomson scattering system*. Rev. Sci. Instrum. **81** (10E131).2010
- [13] R.D. Smirnov et al., *On visibility of carbon dust particles in fusion plasmas with fast framing cameras*. Plasma Phys. Control. Fusion **51** (055017), 2009
- [14] R.D. Smirnov et al., *Laser-dust interaction and dust size distribution measurements on DIII-D*. Phys. Plasmas 14 (112507), 2007